# Mechanical Reinforcement of Epoxy with Self-Assembled Synthetic Clay in Smectic Order

**8 AUTHORS**, INCLUDING:

Kevin L. White
Kyushu University
**31** PUBLICATIONS **128** CITATIONS

Zhengfa Chen
University of Kansas
**9** PUBLICATIONS **30** CITATIONS

Daehak Kim
University of Houston
**3** PUBLICATIONS **18** CITATIONS

Ramanan Krishnamoorti
University of Houston
**190** PUBLICATIONS **8,553** CITATIONS

# Mechanical Reinforcement of Epoxy with Self-Assembled Synthetic Clay in Smectic Order

Peng Li,[†] Kevin L. White,[‡,#] Chien-Hong Lin,[‡] Daehak Kim,[§] Anastasia Muliana,[‡] Ramanan Krishnamoorti,[§] Riichi Nishimura,[‖] and Hung-Jue Sue*[,†,‡]

[†]Department of Materials Science and Engineering and [‡]Department of Mechanical Engineering, Texas A&M University, College Station, Texas 77843, United States

[§]Department of Chemical and Biomolecular Engineering, University of Houston, Houston, Texas 77204, United States

[‖]Corporate R&D Division, Kaneka Corporation, Osaka 530-8288, Japan

**S** *Supporting Information*

**ABSTRACT:** Epoxy films containing self-assembled 2D colloidal $\alpha$-zirconium phosphate nanoplatelets (ZrP) in smectic order were prepared using a simple, energy-efficient fabrication process suitable to industrial processing. The ZrP nanoplatelets form a chiral smectic mesophase with simultaneous lamellar order and helical arrangements in epoxy. The epoxy nanocomposite films are transparent and flexible and exhibit exceptionally high tensile modulus and strength. The findings have broad implications for development of multifunctional materials for engineering applications.



**KEYWORDS:** *liquid crystals, smectic mesophase, ZrP nanoplatelets, tensile properties*
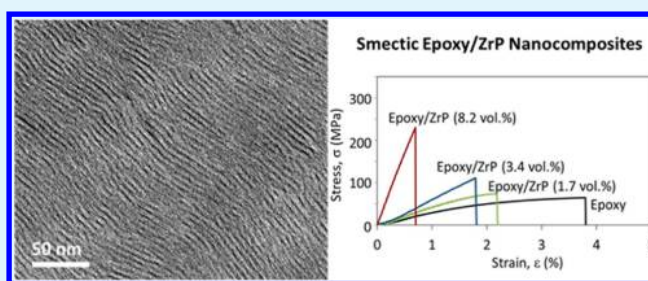
## 1. INTRODUCTION

Polymer/clay nanocomposites have received tremendous attention in recent years due to their low cost, excellent performance at much lower concentrations than needed with conventional, micrometer-diameter fillers, and potential for expanding the application space of polymers.[1−6] However, there remain significant challenges to achieving high-volume production of high-performance polymer/clay nanocomposites for commercial applications, particularly due to current limitations in the incorporation of high levels of clay in polymer matrices without causing clay agglomeration or requiring sophisticated and energy-intensive sample preparation steps.[3] Biological materials such as nacre (mother-of-pearl) have outstanding strength and stiffness due to their robust brick-and-mortar architecture, which consists of alternating layers of soft proteins and aligned calcium carbonate platelets.[7] The mechanical performance of polymer/clay nanocomposites may potentially be significantly improved by achieving similar architecture.[8,9] Transferring these highly regular and organized structures into a structural polymeric system will yield commercially viable materials suitable for a variety of high-performance engineering applications, such as lightweight vehicles, high-performance packaging materials, aerospace structures, and biomedical implants, but must be achieved in an efficient and a scalable manner.[10]

A number of different inorganic reinforcing platelets have been used for fabrication of high-performance polymer nanocomposites, such as graphene, graphene oxide (GO), silicon carbide, talc, mica, and clay.[11−14] Significant improvements in stiffness and strength have been achieved at rather low nano-filler concentrations, particularly in the case of polymer nanocomposites reinforced with high aspect ratio, exfoliated clay nanoparticles.[2,15] Nevertheless, improvements in strength and modulus at high clay concentrations are still notably lower than those anticipated based on theoretical models for reinforced polymers.[15] The limitations are mainly attributed to difficulties in achieving a high volume fraction of well-dispersed and highly ordered nanoplatelets in polymer matrices without nanoplatelet agglomeration.[16]

Several assembly techniques have been developed to achieve the brick-and-mortar structure and corresponding mechanical properties of biological composites, such as layer-by-layer (LbL) assembly, ice templating and sintering of ceramics, air/water interface assembly, vacuum filtration assembly, and electrophoretic deposition.[17−21] Kotov et al.[7] used LbL assembly to fabricate a poly(vinyl alcohol) (PVA) hybrid film containing 50 vol % montmorillonite (MMT) that showed an exceptionally large tensile strength of 400 MPa and Young's modulus of 106 GPa. The tensile properties greatly exceed those of natural nacre, which has a tensile strength of 140−170 MPa and Young's modulus of 60−70 GPa.[22] Using controlled freeze casting of ceramic aqueous suspensions, Ritchie et al.[18] designed a poly(methyl methacrylate) (PMMA) film containing aluminum oxide platelets and observed lamellar organization.

At a concentration of 80 vol % aluminum oxide, the tensile strength of the composite was reported to be 200 MPa.

Most previous approaches for preparing highly aligned lamellar structures have been based on time-consuming sequential deposition methods or require extensive energy consumption. These approaches are limited in scale and often highly specific to certain polymer/clay systems. Recently, Ikkala et al.[10] developed a simple self-assembly approach to fabricate PVA/clay films with lamellar-like order and reported a Young's modulus of 45 GPa. Das et al.[40] reported a further simplified self-assembly approach using sodium carboxymethyl cellulose and MMT. However, the fabrication techniques typically require the use of water-soluble polymers, which results in composite materials with poor robustness and properties that depend on environmental conditions and are generally unsuitable for engineering applications in humid environments. Significant efforts have been focused on improving the mechanical performance of waterborne polymer/clay nano-composites at high humidity condition, with some recent success reported using covalent cross-linking and ionic supramolecular bonding.[7,9,55] Novel methodologies that are able to transfer well-defined nanoscale building blocks into engineering polymers in a simple, practical, and scalable manner remain highly desirable.

In this work, $\alpha$-zirconium phosphate (ZrP) nanoplatelets, which are synthetic crystals with analogous structure to natural clay platelets, were selected to reinforce epoxy matrix. ZrP nanoplatelets can synthesized with well-controlled size and are easily exfoliated in epoxy. We recently reported that ZrP nanoplatelets self-assemble into a smectic mesophase in various solvents[27,54] and retain highly aligned lamellar organization in epoxy matrix.[56] Here, epoxy nanocomposites containing up to 8.2 vol % ZrP were cast into films via a simple film fabrication process. The liquid crystal structure and mechanical properties are reported. The approach presented here is a simple and an effective method to prepare mechanically strong epoxy nanocomposite films suitable for high-performance engineering applications.

## 2. EXPERIMENTAL SECTION

**Materials.** Zirconyl chloride ($ZrOCl_2 \cdot 8H_2O$, 98%, Aldrich) and phosphoric acid (85%, EM Science) were used as received. Bisphenol F epoxy (Epon 862) and curing agent (Epikure W) were purchased from Momentive (Columbus, OH). A commercial polyoxyalkylene-amine, Jeffamine M1000, was obtained from Huntsman Chemical Corp. (The Woodlands, TX).

**Synthesis and Exfoliation of ZrP Nanoplatelets.** ZrP nano-platelets were synthesized using a previously reported refluxing method.[23] Briefly, 15 g of zirconyl chloride ($ZrOCl_2 \cdot 8H_2O$) was refluxed in 150 mL of 3.0 M $H_3PO_4$ for 24 h at 100 °C. The recovered ZrP product was washed three times with deionized (DI) water through centrifugation and redispersion, dried at 65 °C in an oven for 24 h, and then gently ground into a fine powder with a mortar and pestle. ZrP nanoplatelets were exfoliated with a commercial mono-amine intercalating agent (Jeffamine M1000) in acetone.[24]

**Preparation of Epoxy/ZrP Thin Films.** Five grams of bisphenol-F epoxy was dissolved in 10 mL of acetone. The epoxy solution was added dropwise to the acetone/ZrP dispersion (20 mg/mL) under stirring to achieve the desired ZrP concentration. The dispersion was allowed to stir for 6 h. An aromatic amine (Epikure W) curing agent was added at a stoichiometric ratio and homogenized by mechanical mixing. After the solvent was removed with a rotary evaporator, the epoxy/ZrP liquid was B-stage cured for 90 min at 110 °C and subsequently coated on release paper (donated by Hexcel Company) using an Elcometer 4340 (Rochester Hills, MI) thin film applicator.[33]

The coating speed and substrate temperature were controlled to obtain a uniform film with a desired thickness of about 20 $\mu$m. Thin films were cured at 90 °C for 1 h, 120 °C for 1 h, 177 °C for 3 h, and 190 °C for 5 h to prepare fully cured epoxy/ZrP nanocomposite films.

**Characterization.** Transmission electron microscopy (TEM) was performed using a JEOL 2010 high-resolution transmission electron microscope operating at an accelerating voltage of 200 kV. X-ray diffraction (XRD) patterns were obtained using a Bruker D8 Advanced Powder X-ray diffractometer with Cu K$\alpha$ incident radiation ($\lambda$ = 1.5418 Å). Scanning electron microscopy (SEM) and energy-dispersive spectroscopy (EDS) were carried out using a JEOL JSM-7500F Field Emission-SEM (FE-SEM). Optical micrographs (OM) were collected using an Olympus BX60 optical microscope. Circular dichroism (CD) spectra were acquired using a JASCO J-710 CD-spectrometer. Grazing-incidence small-angle X-ray scattering (GISAXS) and small-angle X-ray scattering (SAXS) experiments were performed using a Rigaku S-Max 3000 at the University of Houston. GISAXS data was collected at a grazing incidence angle of 0.05° (Cu K$\alpha$ radiation, $\lambda$ = 1.54056 Å). Tensile tests and dynamic mechanical analysis were conducted using an RSA-G2 (TA Instruments) with a tensile fixture. Tensile tests were conducted in controlled strain mode with a constant linear rate of 0.05 mm/s. The temperature dependence of the linear viscoelastic moduli was determined by applying an oscillatory shear at an angular frequency of $\omega$ = 6.28 rad/s and increasing temperature at a rate of 1 °C/min. The rheological behavior was measured using an ARES-G2 strain-controlled rota-tional rheometer (TA Instruments) using a parallel plate fixture with 40 mm diameter plates.

The volume fraction of ZrP in epoxy was calculated from the mass fraction of ZrP, which was determined using a TA Instruments Q500 thermogravimetric analyzer (TGA). Samples were heated to 800 °C in air at a heating rate of 10 °C/min and held for 10 min to obtain a solid residue of zirconium pyrophosphate ($ZrP_2O_7$). The equivalent ZrP mass fraction was determined using a stoichiometric ratio of $ZrP_2O_7/ZrP$ = 0.88. The mass fraction was converted to volume fraction using $v_i = m_i/\rho_i / \sum m_i/\rho_i$, where $\rho_i$ and $m_i$ are the density and mass fraction of each component in the nanocomposite, respectively.

## 3. RESULTS

Epoxy nanocomposite films containing ZrP nanoplatelets in smectic order were prepared via a simple film fabrication process (Figure 1). ZrP nanoplatelets have a number of distinct
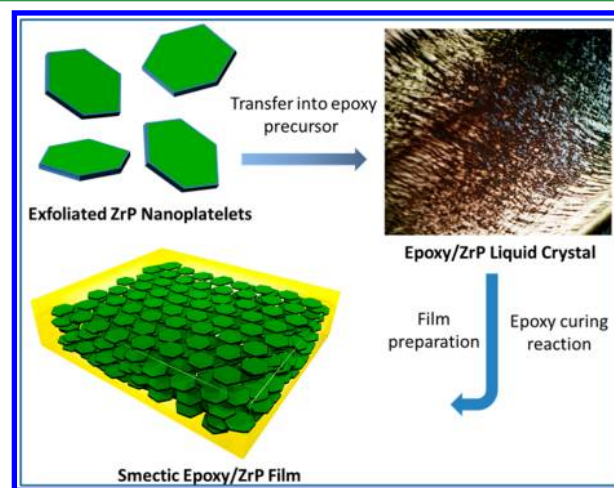


**Figure 1.** Scheme of the preparation process of smectic epoxy/ZrP film.

advantages that make it a useful "model" nanoparticle for fundamental study. In particular, the simple and flexible synthesis route allows preparation of ZrP nanoplatelets with well-controlled diameter, high crystallinity, relatively narrow

size distribution, well-defined chemical structure, high purity, and facile exfoliation of as-synthesized tactoids into individual nanoplatelets.[23,24] The hexagonal ZrP nanoplatelets have an average diameter of 110 nm (Figure 2) and monodisperse
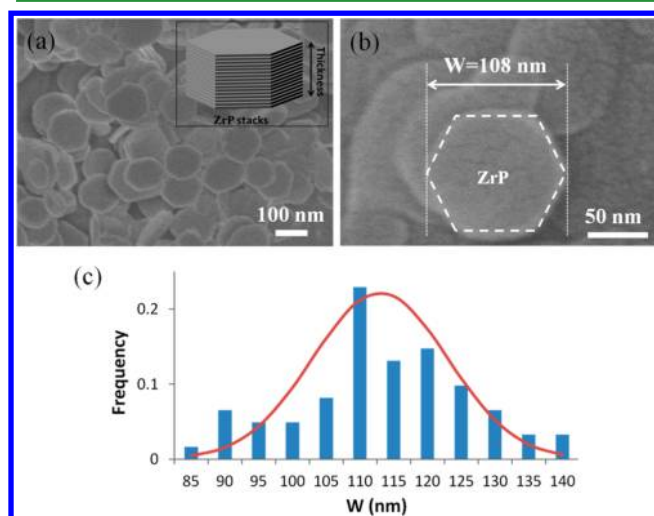


**Figure 2.** (a, b) SEM images and (c) size distribution of as-prepared ZrP nanoplatelets.

thickness of about 0.69 nm.[25] The aspect ratio of the as-prepared ZrP nanoplatelets is approximately 160.

According to Onsager's theory,[26] high aspect ratio particles tend to form liquid crystal phases above a critical volume fraction due to a net gain in entropy as the loss of orientational entropy is compensated by an increase in translational entropy. We recently reported that ZrP exfoliated with M1000 oligomers self-assemble into a long-range liquid crystal mesophase over a range of volume fraction from 0.017 to 0.053 in epoxy.[56] In this work, we were able to prepare high-quality films with concentrations up to 8.2 vol % ZrP. To determine the impact of the increase in concentration of ZrP on processability, rheological measurements were carried out on the epoxy/ZrP suspensions without curing agent. The smectic epoxy/ZrP liquids show high viscosity at low shear rates but also display an extreme degree of shear thinning. At a shear rate of 100 s$^{-1}$, the viscosity of the highly filled suspensions is on the same order of magnitude as the unfilled epoxy fluid. The extreme shear thinning is similar to previous observations[56] and attributed to the sliding of ZrP nanoplatelets within self-assembled smectic layers. The liquid crystal behavior of epoxy/ZrP liquid before addition of curing agent was investigated using cross-polarized light OM (Figure 3a). At 8.2 vol % ZrP, the suspension shows band-like birefringent features that are similar to Grandjean textures associated with a twisted-grain-boundary (TGB) phase.[28] The optical texture confirms that there is long-range organization of the ZrP nanoplatelets into a liquid crystalline mesophase. The bands suggest that that there is a helical arrangement of nanoparticles within the smectic liquid crystalline phase.

The microstructure of the epoxy/ZrP liquids was quantitatively investigated using SAXS and CD measurements. SAXS measurements on suspensions containing 8.2 vol % ZrP show a strong anisotropic scattering pattern that suggests lamellar organization of ZrP in epoxy (Figure 3b and 3c). A characteristic CD spectrum of the epoxy/ZrP liquid spans from 400 to 570 nm (Figure 3d), which indicates a helical arrangement
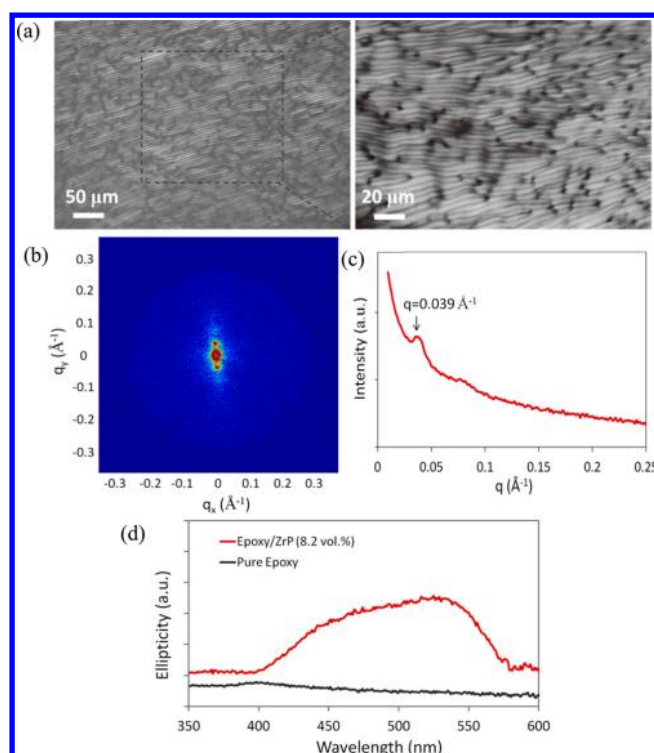


**Figure 3.** (a) Cross-polarized light OM at two magnifications, (b, c) SAXS 2D and 1D diffractograms of smectic epoxy/ZrP (8.2 vol %), and (d) CD spectra of pure epoxy and epoxy/ZrP (8.2 vol %) liquids.

of ZrP. Fully cured epoxy/ZrP thin films were prepared using a simple coating method. Optical images of a self-supporting epoxy/ZrP (8.2 vol %) nanocomposite film are shown in Figure S1(a,b), Supporting Information. The film is transparent and shows significant mechanical robustness and flexibility. The film has an average thickness of 23 $\mu$m (Figure S1(c), Supporting Information), and EDS elemental mapping shows that the ZrP is uniformly distributed throughout the cross-section of the film (Figure S1 (d–f), Supporting Information).

XRD patterns of pristine ZrP and exfoliated epoxy/ZrP films at different ZrP concentrations are shown in Figure 4. The
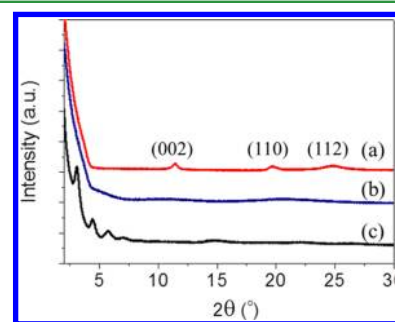


**Figure 4.** XRD spectra of (a) pristine ZrP powder and (b and c) exfoliated epoxy/ZrP nanocomposite films at 3.4 and 8.2 vol % of ZrP, respectively.

pristine ZrP displays a peak at 0.76 nm that corresponds to the (002) diffraction plane (Figure 4a). The epoxy/ZrP nanocomposite containing 3.4 vol % ZrP shows no distinct peaks, which indicates that the nanoplatelets are exfoliated. The broad hump corresponds to the amorphous epoxy matrix (Figure 4b). The epoxy containing 8.2 vol % ZrP shows diffraction peaks

10190

dx.doi.org/10.1021/am5015293 | ACS Appl. Mater. Interfaces 2014, 6, 10188−10195

that confirm the presence of a smectic phase with an interlayer distance of 3.3 nm (Figure 4c). TEM was also carried out to verify the organization of the ZrP in the epoxy (Figure 5).
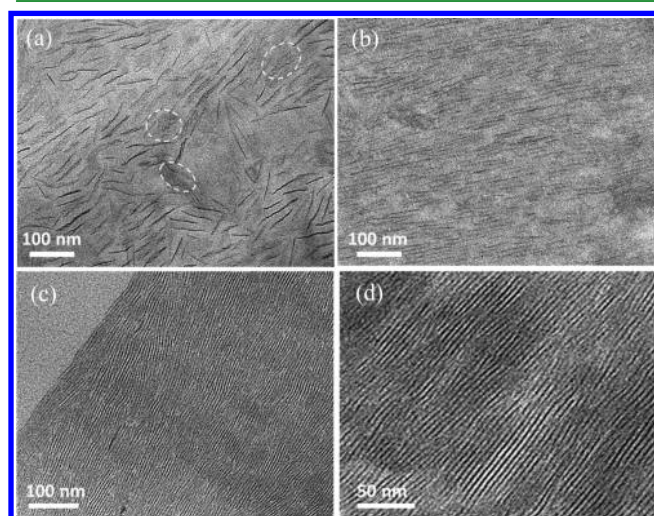


**Figure 5.** TEM images of epoxy/ZrP nanocomposite films at various ZrP concentrations: (a) 1.7, (b) 3.4, and (c, d) 8.2 vol %. ZrP nanoplatelets oriented parallel to the TEM section are indicated by white dotted cycles.

The ZrP nanoplatelets are well dispersed in the epoxy matrix and show no evidence of aggregation. At 8.2 vol % ZrP, the nanoplatelets are self-assembled into a well-aligned mesoscopic structure.

The mesoscale structure of the thin films was investigated using GISAXS.[29,57−59] Lamellar structures aligned parallel to the film surface will display Bragg peaks along the $q_z$ axis. Peaks appearing along the $q_x$ axis correspond to a perpendicular alignment with respect to the film surface. At lower concentration, Bragg peaks corresponding to lamellar organization are not observed for the epoxy/ZrP films (Figure 6a and 6b).
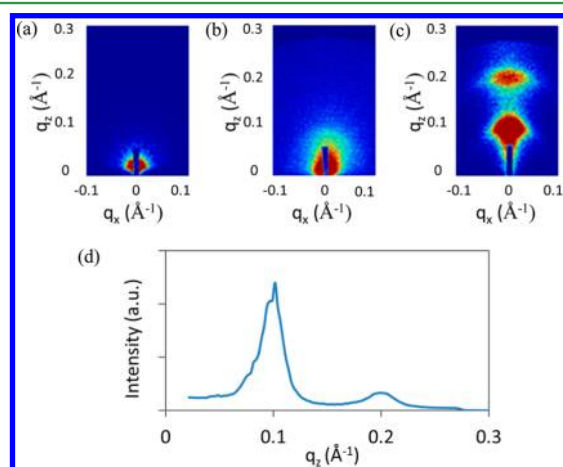


**Figure 6.** GISAXS 2D diffractograms of epoxy/ZrP nanocomposite films at (a) 1.7, (b) 3.4, and (c) 8.2 vol % ZrP. (d) GISAXS 1D diffractogram of epoxy/ZrP (8.2 vol %) film.

GISAXS measurements of the epoxy/ZrP (8.2 vol %) film show first- and second-order Bragg peaks that indicate the presence of a lamellar phase aligned exclusively along the $q_z$ axis (Figure 6c and 6d), i.e., parallel to the film surface.

Tensile stress−strain curves of the neat epoxy and epoxy/ZrP films at several concentrations are shown in Figure 7 and
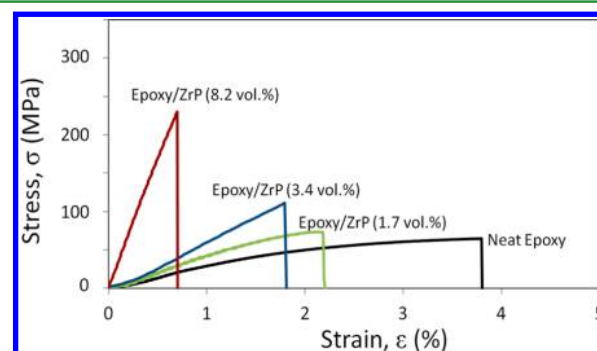


**Figure 7.** Tensile behavior of neat epoxy and epoxy/ZrP nanocomposite films containing different concentrations of ZrP.

summarized in Table 1. The Young's modulus and tensile strength of the nanocomposites increase strongly with ZrP

**Table 1. Tensile Properties of Epoxy/ZrP Films at Various ZrP Concentrations**

|  | neat epoxy | epoxy/ZrP (1.7 vol %) | epoxy/ZrP (3.4 vol %) | epoxy/ZrP (8.2 vol %) |
|---|---|---|---|---|
| Young's modulus, GPa | 2.7 ± 0.4 | 4.4 ± 0.9 | 8.1 ± 2.3 | 22.0 ± 4.0 |
| tensile strength, MPa | 55 ± 5 | 79 ± 9 | 135 ± 25 | 210 ± 40 |
| elongation at break, % | 3.8 ± 0.5 | 2.1 ± 0.3 | 1.6 ± 0.3 | 0.8 ± 0.2 |

concentration. The epoxy/ZrP (8.2 vol %) film shows the most significant improvements in Young's modulus and tensile strength, which are 22 GPa and 210 MPa, respectively. The elongation at break decreases with increasing concentration of ZrP nano-platelets. Nacre-mimetic poly(vinyl alcohol)/montmorillonite nanocomposite films show a similar trend as reported by Kotov et al.[7] Various parameters may be responsible for the change in ductility, such as the mobility of polymer chains, the cross-linking density of network, and the interaction between polymer and nanoplatelets. The decrease in elongation at break suggests that the nanoplatelets lack any mode for cooperative interaction suitable to relieve the build up of local stresses in the epoxy.[33,62]

The dynamic mechanical behavior of the epoxy/ZrP films is shown in Figure 8a. At 35 °C, the tensile storage moduli ($E'$) of the epoxy/ZrP films containing 3.4 and 8.2 vol % ZrP nanoplatelets are 6 and 19 GPa, respectively. The $T_g$ of the films at 3.4 and 8.2 vol % ZrP are 89 and 85 °C, respectively, which are lower than the neat epoxy (148 °C). The reduction in $T_g$ may potentially be attributed to unintended side reactions and/or steric hindrance between the surface-attached mono-amine oligomers and the epoxy monomers.[30]

## 4. DISCUSSION

The results presented here show that at 8.2 vol %, the high aspect ratio ZrP nanoplatelets have self-assembled into a helical smectic liquid crystal mesophase in epoxy. The polarized OM results suggest that the structure is similar to a TGB phase (Figure 3a). The TGB phase was first predicted to occur between cholesteric and smectic A phases by Renn and Lubensky.[31] They proposed that it is impossible to produce a continuous structure that exhibits both a cholesteric director field and a smectic layer structure at the same time. The competition between these two structural features results in discrete grain
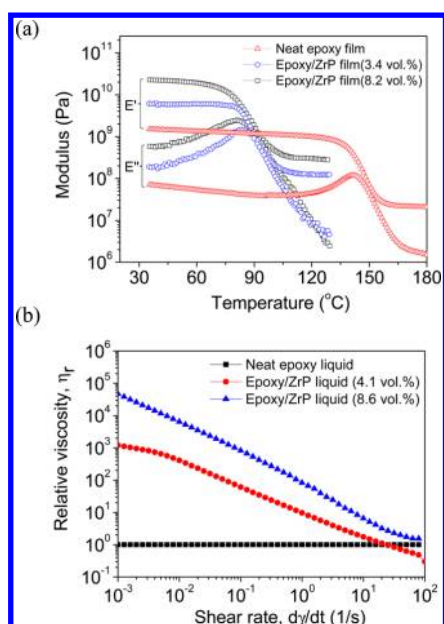
10191

dx.doi.org/10.1021/am5015293 | *ACS Appl. Mater. Interfaces* 2014, 6, 10188−10195

**Figure 8.** (a) DMA spectra of neat epoxy and epoxy/ZrP nanocomposite films. (b) Steady shear viscosity as a function of shear rate for unfilled epoxy and epoxy/ZrP suspensions without curing agent measured at 25 °C.

boundaries that consist of screw dislocations. Experimental observations of a TGB-like phase in aqueous dispersions of GO have been recently reported by Gao et al.[32] To our knowledge, there have been few reports of systems containing plate-like fillers that can self-organize into a helical smectic mesophase in polymer. Unveiling the nature of these mesoscopic structures will enrich our understanding of colloidal liquid crystal formation, which may in turn enhance our ability to prepare novel advanced materials.

On the basis of the OM, SAXS, and CD results, we propose a twisted-lamellar-block model to account for the helical smectic liquid crystalline order of the ZrP nanoplatelets (Figure 9).
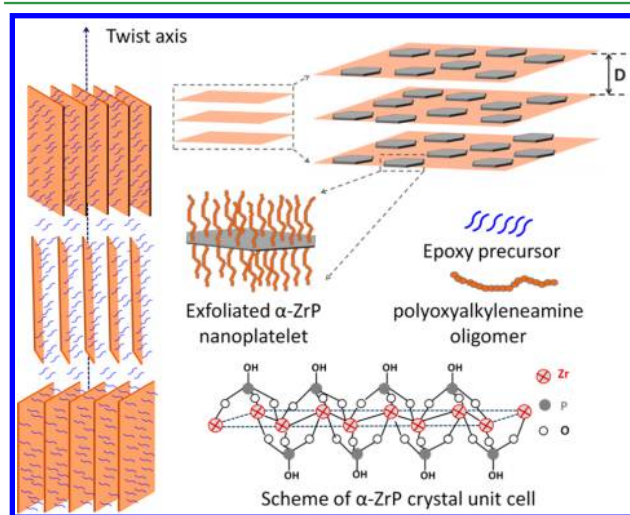


**Figure 9.** Proposed twisted-lamellar-block model to account for the helical smectic liquid crystalline order of the ZrP nanoplatelets in epoxy liquids.

In this model, the grain boundaries of oligomer-modified ZrP blocks produce helical dislocations within the lamellar phase.

The steric hindrance provided by the surface-attached oligomeric brush layer is believed to be the dominant force acting between ZrP nanoplatelets that contributes to formation of lamellar blocks. At the grain boundaries of the ZrP lamellar blocks, the neighboring blocks repel each other and form a rotated conformation through turning to a certain angle to minimize free energy. Since the present data is not sufficient to conclude whether the helical rotation of the ZrP smectic blocks actually occurs in the discrete manner as predicted by the TGB theory,[31] we will refer to the present helical smectic ZrP liquid crystal as a TGB-like structure.

The ZrP nanoplatelets are able to easily self-assemble into well-aligned mesoscopic structures at high ZrP concentrations using the simple nanocomposite fabrication scheme reported here. As shown, a low fraction of ZrP (1.7 vol %) in epoxy only results in random orientation (Figure 5a). As the concentration of ZrP nanoplatelets increases, the frequency of ZrP misalignment appears to proportionally decrease. The population of ZrP nanoplatelets oriented parallel to the TEM thin-section surface (highlighted in Figure 5a) also appears to be higher for lower ZrP concentration systems. These phenomena show the importance of "excluded volume" effects on self-assembly of ZrP and suggest that as ZrP concentration increases, the degree of order of ZrP nanoplatelets in the epoxy matrix progressively increases (Figure 5b and 5c).

One challenge to fabricating polymer nanocomposites at high filler concentrations is that there is often a drastic increase in viscosity that compromises processability. The smectic epoxy/ZrP liquids display extreme shear thinning behavior (Figure 8b). The mechanism responsible for the unique rheological behavior of the smectic liquid crystalline systems was recently reported by White et al.[35] and attributed to concentration-dependent interactions between monoamine tethered ZrP nanoplatelets. The extreme shear thinning property allows bulk polymer nanocomposites to be prepared with a high volume fraction of nanoplatelets using a simple fabrication process. Controlling the long-range organization of high aspect ratio nanoparticles is a useful method for preparation of high nanofiller content polymer nanocomposites without compromising processability.

The epoxy/ZrP films with smectic order show greatly improved mechanical properties (Table 1). The epoxy/ZrP (8.2 vol %) film shows significantly improved Young's modulus compared to the neat epoxy. The remarkable mechanical stiffness (22 GPa) is among the best reported properties for nacre-inspired composites and was achieved at relatively low concentration.[40] Previous work[7] has attributed limited improvements in mechanical reinforcement of polymer/clay composites at high filler concentrations to difficulties in achieving good dispersion of the nanoplatelets and well-controlled microstructure at the mesoscale. Clay has a strong tendency to aggregate and phase separate at high loadings due to mutually strong attractive interactions.[30] It is possible to produce high-performance nanocomposites with well-controlled spatial and orientational alignment of clay platelets by manipulating colloidal interactions.[36] Furthermore, load transfer between nanoplatelets and the polymer matrix is largely determined by the interfacial bonding between the two constituents.[7] The ZrP nanoplatelets possess P−OH Brønsted acid groups in the interlayer region and readily undergo intercalation reactions with proton-accepting functional groups, such as amines.[24] The hydroxyl-terminated functional groups on the ZrP surface may be able to form hydrogen bonds with the oxygen atoms in the epoxy backbone, which would improve interfacial cohesion.

The well-controlled microstructural organization of the clay platelets in the nanocomposites will also maximize the total surface area between the epoxy and ZrP, which will further enhance load transfer efficiency between the stiff inorganic platelets and the soft polymer matrix.

The tensile properties of the epoxy/ZrP films prepared here are summarized in Figure S2, Supporting Information, and compared with previous reports of polymer/clay films with lamellar-like organization that were prepared using different fabrication techniques. To meaningfully compare the change in modulus and strength with other works, we normalized the modulus and strength by filler volume fraction, given by $dE/dV_f$ and $dS/dV_f$, respectively (Figure 10).[37] The $dE/dV_f$ and $dS/dV_f$
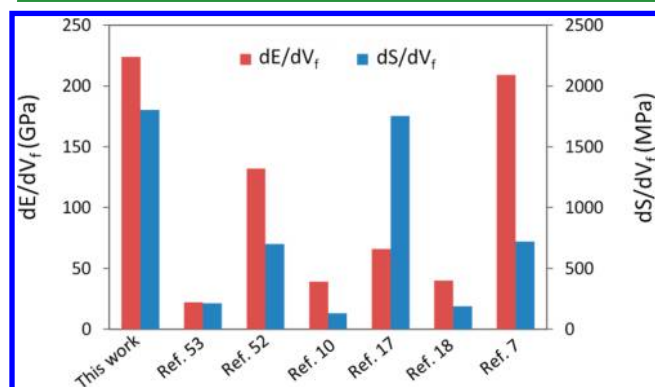


**Figure 10.** $dE/dV_f$ and $dS/dV_f$ of the smectic epoxy/ZrP nanocomposite films and other previously reported polymer/clay films with lamellar-like organization.

of our smectic epoxy/ZrP (8.2 vol %) film are 224 and 1.80 GPa, respectively. These values are among the highest values reported for clay-reinforced polymer nanocomposites.[15,34,38,60,61]

The concentration of nanoparticles is a key factor in determining optimal performance for synthetic bioinspired composites. Natural nacre exhibits a brick-and-mortar architecture that contains ~90 vol % $CaCO_3$ hard platelets within a soft protein matrix. Most nacre-mimetic films prepared by LbL or other self-assembly techniques have focused on maximizing inorganic content and generally achieve loadings of more than 50 wt %.[7,10,18,20,39] However, it has been proposed that extremely high loadings of clay in biomimetic structures may prevent optimal mechanical performance. Walther et al.[40] recently studied the nacre-mimetic films based on carboxymethyl cellulose/clay system and found that the nanocomposite film at 20 wt % of clay loading showed the best combination of mechanical properties with a Young's modulus of ~22 GPa and tensile strength of ~320 MPa. At higher loadings of clay, the tensile properties of nanocomposite films show a decreasing trend. The authors propose that high clay loadings do not allow for sufficient deformation of carboxymethyl cellulose to attain optimal tensile properties. In this work, the epoxy/ZrP nanocomposites containing three different ZrP loadings show different degrees of alignment level (Figures 5 and 6). The maximum concentration was limited to 8.2 vol % ZrP. At higher concentration it is challenging to efficiently remove air bubbles and obtain a uniform film due to the significantly increased viscosity. Other reports have been able to achieve significantly higher concentrations following more complex processing methods, such as layer-by-layer deposition, and usually do not involve thermosetting materials. For the epoxy/ZrP system investigated here, it

may be possible to achieve higher concentrations by modifying the processing conditions and potentially taking greater advantage of the extreme shear thinning behavior (Figure 8b) observed, but this is outside the scope of this work.

The epoxy/ZrP film tensile properties were also compared to theoretical micromechanical model predictions.[41−43] Several popular micromechanical models based on estimation of effective properties were considered (e.g., dilute, Mori-Tanak,a and self-consistent models), along with upper and lower bound predictions. The rationale of each micromechanical model is discussed in detail by Qu et al.[45] The modulus of a single ZrP nanoplatelet is assumed to be 270 GPa.[46] The predictions of the normalized Young's modulus in the radial direction ($E_{11}/E_m$) are shown in Figure 11, where $E_{11}$ and $E_m$ are the moduli
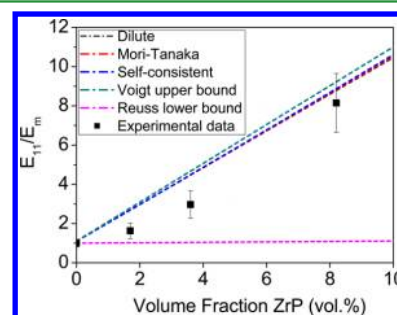


**Figure 11.** Experimental data and micromechanical predictions of Young's modulus in the radial direction ($E_{11}$), shown as functions of platelet volume fraction. Values normalized by Young's modulus of unfilled matrix ($E_m$).

of the nanocomposite and the neat epoxy matrix, respectively. At high ZrP concentration, the experimental findings are in good agreement with the micromechanical predictions, implying that the mechanical properties of the epoxy nanocomposites at 8.2 vol % ZrP loading is near the maximum achievable level based on additive contributions of the individual phases. At lower ZrP loadings, the micromechanical predictions are significantly greater than the observed mechanical performance, which is primarily attributed to the greater degree of ZrP misalignment at lower concentration.

The mechanically strong epoxy/ZrP films prepared in this study have potential applications for many high-performance structural composites and devices. For example, there is significant demand for high-performance polymer nanocomposites as lightweight structural components, barrier films, anticorrosion coatings, fire-retardant materials, and photovoltaic packaging applications.[47−53] Various other plate-like materials such as graphene and its derivatives have been observed to show lamellar organization in solvents[44,63] and may potentially be used in a smilar way to develop functional nanocomposites with excellent mechanical properties. However, large-scale fabrication of solid polymers containing a nanoparticle phase with smectic organization remains to be a challenge. Future efforts will focus on probing the feasibility of using natural and synthetic nanoplatelets with long-range liquid crystalline order in polymer matrices for high-performance applications.

## 5. CONCLUSION

A simple and an effective self-assembly approach has been developed to fabricate epoxy nanocomposite films containing ZrP nanoparticles in smectic order. The high aspect ratio ZrP

nanoplatelets form a chiral smectic mesophase in epoxy with simultaneous lamellar order and helical arrangement. Rheological studies of the epoxy/ZrP liquids show extreme shear thinning at a moderate shear rate and demonstrate that polymer nanocomposites with high filler content may be prepared without compromising processability. Long-range orientational and positional arrangement of ZrP nanoplatelets in smectic order is readily observed in epoxy nanocomposite films, which show exceptional tensile properties with Young's modulus and tensile strength as high as 22 GPa and 210 MPa, respectively, at 8.2 vol % ZrP. Such high-performance epoxy nanocomposites are suitable for large-volume engineering applications.

## ■ ASSOCIATED CONTENT

### Ⓢ Supporting Information

Optical images, SEM and EDS of smectic epoxy/ZrP film, and comparison of tensile properties with lamellar-like nanocomposites. This material is available free of charge via the Internet at http://pubs.acs.org.

## ■ AUTHOR INFORMATION

### Corresponding Author
*E-mail: hjsue@tamu.edu.

### Present Address
[#]International Institute for Carbon-Neutral Energy Research (WPI-I[2]CNER), Kyushu University, Fukuoka 819-0395, Japan.

### Notes
The authors declare no competing financial interest.

## ■ ACKNOWLEDGMENTS

## ■ REFERENCES

(1) Ebina, T.; Mizukami, F. Flexible Transparent Clay Films with Heat-Resistant and High Gas-Barrier Properties. *Adv. Mater.* **2007**, *19*, 2450−2453.

(2) Fornes, T.; Paul, D. R. Modeling Properties of Nylon 6/Clay Nanocomposites using Composite Theories. *Polymer* **2003**, *44*, 4993−5013.

(3) Lee, H.; Fasulo, P.; Rodgers, W.; Paul, D. R. TPO based Nanocomposites. Part 1. Morphology and Mechanical Properties. *Polymer* **2005**, *46*, 11673−11689.

(4) Phua, S.; Yang, L.; Toh, C.; Lau, S.; Dasari, A.; Lu, X. Simultaneous Enhancements of UV Resistance and Mechanical Properties of Polypropylene by Incorporation of Dopamine-Modified Clay. *ACS Appl. Mater. Interfaces* **2013**, *5*, 1302−1309.

(5) Kim, Y.; Li, Y.; Pitts, W.; Werrel, M.; Davis, R. Rapid Growing Clay Coatings to Reduce the Fire Threat of Furniture. *ACS Appl. Mater. Interfaces* **2014**, *6*, 2146−2152.

(6) Dou, Y.; Xu, S.; Liu, X.; Han, J.; Yan, H.; Wei, M.; Evans, D.; Duan, X. Flexible Films Based on Layered Double Hydroxide/Cellulose Acetate with Excellent Oxygen Barrier Property. *Adv. Funct. Mater.* **2014**, *24*, 514−521.

(7) Podsiadlo, P.; Kaushik, A.; Arruda, E.; Shim, B.; Xu, J.; Ramamoorthy, A.; Kotov, N. Ultrastrong and Stiff Layered Polymer Nanocomposites. *Science* **2007**, *318*, 80−83.

(8) Verho, T.; Walther, A.; Ikkala, O. Hydration and Dynamic State of Nanoconfined Polymer Layers Govern Toughness in Nacre-mimetic Nanocomposites. *Adv. Mater.* **2013**, *25*, 5055−5059.

(9) Kochumalayil, J.; Morimune, S.; Nishino, T.; Ikkala, O.; Walther, A.; Berglund, L. Nacre-mimetic Clay/Xyloglucan Bionanocomposites: a Chemical Modification Route for Hygromechanical Performance at High Humidity. *Biomacromolecules* **2013**, *14*, 3842−3849.

(10) Walther, A.; Bjurhger, I.; Malho, J.; Ruokolainen, J.; Berglund, L.; Ikkala, O. Large-Area, Lightweight and Thick Biomimetic Composites with Superior Material Properties via Fast, Economic, and Green Pathways. *Nano Lett.* **2010**, *10*, 2742−2748.

(11) Phua, S.; Yang, L.; Toh, C.; Huang, S.; Lau, K.; Mai, Y.; Lu, X. Reinforcement of Polyether Polyurethane with Dopamine-Modified Clay: The Role of Interfacial Hydrogen Bonding. *ACS Appl. Mater. Interfaces* **2012**, *4*, 4571−4578.

(12) May, P.; Khan, U.; Oneill, A.; Coleman, J. Approaching the Theoretical Limit for Reinforcing Polymers with Graphene. *J. Mater. Chem.* **2012**, *22*, 1278−1282.

(13) Pavlidou, S.; Papaspyrides, C. A Review on Polymer Layered Silicate Nanocomposites. *Prog. Polym. Sci.* **2008**, *33*, 1119−1198.

(14) Hu, X.; Xu, Z.; Liu, Z.; Gao, C. Liquid Crystal Self-templating Approach to Ultrastrong and Tough Biomimic Composites. *Sci. Rep.* **2013**, *3*, 2374−2382.

(15) Paul, D. R.; Robeson, L. Polymer Nanotechnology: Nanocomposites. *Polymer* **2008**, *49*, 3187−3204.

(16) Sheng, N.; Boyce, M.; Parks, D.; Rutledge, G.; Abes, J.; Cohen, R. Multiscale Micromechanical Modeling of Polymer/Clay Nanocomposites and the Effective Clay Particle. *Polymer* **2004**, *45*, 487−506.

(17) Bonderer, L.; Studart, A.; Gauckler, L. Bioinspired Design and Assembly of Platelet Reinforced Polymer Films. *Science* **2008**, *319*, 1069−1073.

(18) Munch, E.; Launey, M.; Alsem, D.; Saiz, E.; Tomsia, A.; Ritchie, R. Tough Bio-Inspired Hybrid Materials. *Science* **2008**, *322*, 1516−1520.

(19) Lin, T.; Huang, W.; Jiang, P. Electrophoretic Deposition of Biomimetic Nanocomposites. *Electrochem. Commun.* **2009**, *11*, 14−17.

(20) Podsiadlo, P.; Michel, M.; Critchley, K.; Srivastava, S.; Qin, M.; Lee, J.; Verploegen, E.; Hart, A.; Qi, Y.; Kotov, N. Diffusional Self-Organization in Exponential Layer-By-Layer Films with Micro- and Nanoscale Periodicity. *Angew. Chem., Int. Ed.* **2009**, *48*, 7073−7077.

(21) Priolo, M.; Gamboa, D.; Grunlan, J. Transparent Clay Polymer Nano Brick Wall Assemblies with Tailorable Oxygen Barrier. *ACS Appl. Mater. Interfaces* **2010**, *2*, 312−320.

(22) Corni, I.; Harvey, T.; Wharton, J.; Stokes, K.; Walsh, F.; Kwood, R. A Review of Experimental Techniques to Produce a Nacre-like Structure. *Bioinspiration Biomimetics* **2012**, *7*, 31001−31024.

(23) Sun, D.; Chu, C.; Sue, H. J. Simple Approach for Preparation of Epoxy Hybrid Nanocomposites Based on Carbon Nanotubes and a Model Clay. *Chem. Mater.* **2010**, *22*, 3773−3778.

(24) Boo, W.; Sun, L.; Liu, J.; Sue, H. J. Effect of Nanoplatelet Dispersion on Mechanical Behavior of Polymer Nanocomposites. *J. Polym. Sci., Part B* **2007**, *45*, 1459−1469.

(25) Hoppe, R.; Costatino, U.; Dionigi, C.; Schulzekloff, G.; Vivani, R. Intercalation of Dyes in Layered Zirconium Phosphates Preparation and Spectroscopic Characterization of α-Zirconium Phosphate Crystal Violet Compounds. *Langmuir* **1997**, *13*, 7252−7257.

(26) Onsager, L. The Effects of Shape on the Interaction of Colloidal Particles. *Ann. N.Y. Acad. Sci.* **1949**, *51*, 627−659.

(27) Sun, D.; Sue, H. J.; Cheng, Z.; Martinezraton, Y.; Velasco, E. Stable Smectic Phase in Suspensions of Polydisperse Colloidal Platelets with Identical Thickness. *Phys. Rev. E* **2009**, *80*, 41704−41710.

(28) Goodby, J. W.; Waugh, M.; Stein, S.; Chin, E.; Pindak, R.; Patel, J. Characterization of a New Helical Smectic Liquid Crystal. *Nature* **1989**, *337*, 449−452.

(29) Lin, Y.; Smith, K.; Kempf, C.; Verduzco, R. Synthesis and Crystallinity of All Conjugated poly(3-hexylthiophene) Block Copolymers. *Polym. Chem.* **2013**, *4*, 229−232.

(30) Sue, H. J.; Gam, K. T.; Bestaoui, N.; Clearfield, A.; Miyamoto, M.; Miyatake, N. Epoxy Nanocomposites Based on the Synthetic α-Zirconium Phosphate Layer Structure. *Chem. Mater.* **2004**, *16*, 242−249.

(31) Lubensky, T. C.; Renn, S. R. Twist-Grain-Boundary Phases Near the Nematic−Smectic A−Smectic C Point in Liquid Crystals. *Phys. Rev. A* **1990**, *41*, 4392−4401.

(32) Xu, Z.; Gao, C. Graphene Chiral Liquid Crystals and Macroscopic Assembled Fibres. *Nat. Commun.* **2011**, *2*, 571−579.

(33) White, K.; Sue, H. J. Delamination Toughness of Fiber Reinforced Composites Containing a Carbon Nanotube/Polyamide-12 Epoxy Thin Film Interlayer. *Polymer* **2012**, *53*, 37−42.

(34) Weon, J. I.; Sue, H. J. Effects of Clay Orientation and Aspect Ratio on Mechanical Behavior of Nylon-6 Nanocomposite. *Polymer* **2005**, *46*, 6325−6334.

(35) White, K. Rheology of Model Nanoparticle Suspensions in Epoxy. Dissertation, Texas A&M University, TX, USA, 2013.

(36) Mourad, M.; Devid, E.; Schooneveld, M.; Vonk, C.; Lekkerkerker, H. Formation of Nematic Liquid Crystals of Sterically Stabilized Layered Double Hydroxide Platelets. *J. Phys. Chem. B* **2008**, *112*, 10142−10152.

(37) Cadek, M.; Coleman, J. N.; Ryan, K.; Nicolosi, V.; Bister, G.; Fonseca, A. J.; Nagy, K.; Szostak, W. Blau, Reinforcement of Polymers with Carbon Nanotubes: The Role of Nanotube Surface Area. *Nano. lett.* **2004**, *7*, 353−356.

(38) Pavlidoua, S.; Papaspyridesb, C. A Review on Polymer Layered Silicate Nanocomposites. *Prog. Polym. Sci.* **2008**, *33*, 1119−1198.

(39) Walther, A.; Bjurhager, I.; Malho, J. M.; Ruokolainen, J.; Berglund, L.; Ikkala, O. Supramolecular Control of Stiffness and Strength in Lightweight High-Performance Nacre-Mimetic Paper with Fire-Shielding Properties. *Angew. Chem., Int. Ed.* **2010**, *49*, 6448−6453.

(40) Paramita, D.; Schipmann, S.; Malho, J.; Zhu, B.; Klemradt, U.; Walther, A. Facile Access to Large-Scale Self-Assembled Nacre-Inspired High-Performance Materials with Tunable Nanoscale Periodicities. *ACS Appl. Mater. Interfaces* **2013**, *5*, 3738−3747.

(41) Tandon, G. P.; Weng, G. J. The Effect of Aspect ratio of Inclusions on the Elastic Properties of Unidirectionally Aligned Composites. *Polym. Compos.* **1984**, *5*, 327−333.

(42) Mori, T.; Tanaka, K. Average Stress in Matrix and Average Elastic Energy of Materials with Misfitting Inclusions. *Acta Metall. Mater.* **1973**, *21*, 571−574.

(43) Halpin, J. C. Stiffness and Expansion Estimates for Oriented Short Fiber Composites. *J. Compos. Mater.* **1969**, *3*, 732−734.

(44) Li, P.; Yao, H.; Wong, M.; Sugiyama, H.; Zhang, X.; Sue, H. J. Thermally Stable and Highly Conductive Free-standing Hybrid Films based on Reduced Graphene Oxide. *J. Mater. Sci.* **2014**, *49*, 380−391.

(45) Qu, J.; Cherkaoui, M. *Fundamentals of Micromechanics of Solids*; Wiley: Hoboken, NJ, 2006.

(46) Manevitch, O. L.; Rutledge, G. C. Elastic Properties of a Single Lamella of Montmorillonite by Molecular Dynamics Simulation. *J. Phys. Chem. B* **2004**, *108*, 1428−1435.

(47) Ammala, A.; Pas, S.; Lawrence, K.; Stark, R.; Webb, R.; Hill, A. Poly(m-xylene adipamide)-Montmorillonite Nanocomposites Effect of Organo-Modifier Structure on Free Volume and Oxygen Barrier Properties. *J. Mater. Chem.* **2008**, *18*, 911−916.

(48) Nambiar, S.; Yeow, J. Polymer Composite Materials for Radiation Protection. *ACS Appl. Mater. Interfaces* **2012**, *4*, 5717−5726.

(49) Karine, J. C.; Bonino, J.; Gressier, M.; Joelle, M.; Pebere, N. Improvement of Barrier Properties of a Hybrid Sol−Gel Coating by Incorporation of Synthetic Talc-like Phyllosilicates for Corrosion Protection of a Carbon Steel. *Surf. Coat. Technol.* **2012**, *206*, 2884−2891.

(50) Yang, G.; Hou, W.; Feng, X.; Xu, L.; Liu, Y.; Wang, G.; Ding, W. Nanocomposites of Polyaniline and a Layered Inorganic Acid Host Polymerization of Aniline in the Layers Conformation and Electrochemical Studies. *Adv. Funct. Mater.* **2007**, *17*, 401−412.

(51) Zhao, M.; Zhang, Q.; Huang, J.; Wei, F. Hierarchical Nanocomposites Derived from Nanocarbons and Layered Double Hydroxides Properties Synthesis and Applications. *Adv. Funct. Mater.* **2012**, *22*, 675−694.

(52) Wang, J.; Cheng, Q.; Lin, L.; Chen, L.; Jiang, L. Understanding the Relationship of Performance with Nanofiller Content in the Biomimetic Layered Nanocomposites. *Nanoscale* **2013**, *5*, 6356−6362.

(53) Tang, Z.; Kotov, N. A.; Magonov, S.; Ozturk, B. Nanostructured Artificial Nacre. *Nat. Mater.* **2003**, *2*, 413−418.

(54) Wong, M.; Ishige, R.; Hoshino, T.; Hawkins, S.; Li, P.; Takahara, A.; Sue, H. J. Solution Processable Iridescent Self-Assembled Nanoplatelets with Finely Tunable Interlayer Distances Using Charge and Sterically Stabilizing Oligomeric Polyoxyalkyleneamine Surfactants. *Chem. Mater.* **2014**, *26*, 1528−1537.

(55) Das, P.; Walther, A. Ionic Supramolecular Bonds Preserve Mechanical Properties and Enable Synergetic Performance at High Humidity in Water-borne Self-assembled Nacre-mimetics. *Nanoscale* **2013**, *5*, 8348−9356.

(56) Wong, M.; Ishige, R.; White, K.; Li, P.; Kim, D.; Krishnamoorti, R.; Gunther, R.; Higuchi, T.; Jinnai, H.; Takahara, A.; Nishimura, R.; Sue, H. J. Large-scale Self-assembled Zirconium Phosphate Smectic Layers via a Simple Spray-coating Process. *Nat. Commun.* **2014**, doi:10.1038/ncomms4589 (accessed Apr. 7, **2014**).

(57) Müller-Buschbaum, P.; Roth, S. V.; Burghammer, M.; Diethert, A.; Panagiotou, P.; Riekel, C. Multiple-scaled Polymer Surfaces Investigated with Micro-focus Grazing-incidence Small-angle X-ray Scattering. *Europhys. Lett.* **2003**, *61*, 639−645.

(58) Müller-Buschbaum, P.; Bauer, E.; Maurer, E.; Schlögl, K.; Roth, S. V.; Gehrke, R. Route to Create Large-area Ordered Polymeric Nanochannel Arrays. *Appl. Phys. Lett.* **2006**, *88*, 083114−7.

(59) Müller-Buschbaum, P. Grazing Incidence Small-angle X-ray Scattering: an Advanced Scattering Technique for the Investigation of Nanostructured Polymer Films. *Anal. Bioanal. Chem.* **2003**, *376*, 3−10.

(60) Usuki, A.; Kojima, Y.; Kawasumi, M.; Okada, A.; Fukushima, Y.; Kurauchi, T.; Kamigaito, O. Synthesis of Nylon Clay Hybrid. *J. Mater. Res.* **1993**, *8*, 1179−1184.

(61) Usuki, A.; Kato, M.; Okada, A.; Kurauchi, T. Synthesis of Polypropylene Clay Hybrid. *J. Appl. Polym. Sci.* **1997**, *63*, 137−139.

(62) White, K.; Sue, H. J. Electrical Conductivity and Fracture Behavior of Epoxy/Polyamide-12/Multi-walled Carbon Nanotube Composites. *Polym. Eng. Sci.* **2011**, *51*, 2245−2253.

(63) Li, P.; Wong, M.; Zhang, X.; Yao, H.; Ishige, R.; Takahara, A.; Miyamoto, M.; Nishimura, R.; Sue, H. J. Tunable Lyotropic Photonic Liquid Crystal Based on Graphene Oxide. *ACS Photonics* **2014**, *1*, 79−86.

10195

dx.doi.org/10.1021/am5015293 | *ACS Appl. Mater. Interfaces* 2014, 6, 10188−10195